2011 International Symposium on Nonlinear Theory and its Applications
NOLTA2011, Kobe, Japan, September 4-7, 2011

Basic analysis of synchronous phenomena from coupled asynchronous sequential logic neurons

Hirofumi Ijichi† and Hiroyuki Torikai†

†Graduate School of Engineering Science, Osaka University
1-3 Machikaneyama, Toyonaka, Osaka, 560-8351, Japan

Abstract—An asynchronous sequential logic spiking neuron is an artificial neuron model that can exhibit various bifurcations and nonlinear responses to stimulation inputs. In this paper, we introduce a pulse-coupled system of the asynchronous sequential logic spiking neurons. It is shown that the coupled system can exhibit various periodic islands and their synchronization phenomena.

1. Introduction

Designs of artificial spiking neuron models and their pulse-coupled networks that are suitable for electronic hardware implementations have been hot research topics for a long time [1]-[7], where there exit two major approaches as summarized in Table 1: (1) an analog VLSI approach that implements an *ordinary differential equation* (ab. ODE) by a nonlinear analog circuit, and (2) a digital processor approach that implements a numerical integration by a digital processor with a memory. Recently, a novel hardware-oriented neuron modeling approach has been proposed, where the nonlinear dynamics of a neuron is modeled by an asynchronous *cellular automaton* (ab. CA) that is implemented by an asynchronous sequential logic circuit [8]-[11]. Among these asynchronous sequential logic spiking neurons, one of the simplest models is the *integrate-and-type digital spiking neuron* (ab. DSN) [10] that can exhibit various bifurcations and nonlinear responses to input spike-trains.

In this paper, a *pulse-coupled system of the DSNs* (ab. PCDSN) is introduced. It is shown that each DSN can exhibit various periodic islands. It is also shown that the PCDSN can exhibit various synchronization phenomena (lockings) of the islands whose characteristics have similarities to devil's staircases and Arnold tongues. Significances of this paper include the following points. (a) The PCDSN can be easily implemented by a wired system of shift registers, where the wiring pattern (i.e., control parameter) can be easily and dynamically updated by using a reconfigurable hardware such as a dynamic reconfigurable FPGA [12] as summarized in Table 1. (b) Asynchronous CAs and asynchronous sequential logic circuits have not been sufficiently investigated compared to synchronous ones [13][14]. The series of the researches on asynchronous sequential logic spiking neurons (including this paper) [8]-[11] will contribute to develop a research framework of nonlinear dynamics of asynchronous CAs and/or asynchronous sequential logic circuits.

Table 1: Artificial spiking neurons.

Approach	Analog VLSI [1]-[5]	Digital Processor [6][7]	Asynchronous Sequential logic [8]-[11]
Dynamics	Nonlinear ODE	Numerical Integration	Asynchronous CA
State / Time	Continuous / Continuous	Discrete / Discrete	Discrete / Continuous
Implementation	Analog nonlinear circuit	Processor, memory, and peripherals	Wired shift registers (compact sequential logic circuit)
Dynamic parameter update	Straightforward implementation is troublesome	Possible by processor	Possible by dynamic reconfigurable hardware

2. Pulse-Coupled Digital Spiking Neurons and Periodic Synchronization Phenomena

In this section, we introduce a *pulse-coupled system of two digital spiking neurons* (ab. PCDSN) the hardware model of which is shown in Fig.1, where the two digital spiking neurons (ab. DSNs) are denoted by $\mathrm{DSN}^{(1)}$ and $\mathrm{DSN}^{(2)}$. The PCDSN has the following internal clock.

$$C(t) = \begin{cases} 1 & \text{if } t = 0, 1, 2, \cdots, \\ 0 & \text{otherwise,} \end{cases}$$

where $t \in \boldsymbol{R}$ is a continuous time.

First, we explain the dynamics of the $\mathrm{DSN}^{(1)}$. The rhythm register is an $M^{(1)}$-bit one-hot-coded shift register having an integer state $P^{(1)} \in \{0, 1, \cdots, M^{(1)} - 1\}$ called a rhythm state. The internal clock $C(t)$ induces transitions of the rhythm state $P^{(1)}$ as follows.

$$P^{(1)}(t^+) = \begin{cases} P^{(1)}(t) + 1 \pmod{M^{(1)}} & \text{if } C(t) = 1, \\ P^{(1)}(t) & \text{otherwise,} \end{cases} \quad (1)$$

where $t^+ \equiv \lim_{\delta \to +0} t + \delta$. The rhythm register is wired to the $N^{(1)}$-bit membrane register, where the wiring pattern is described by the following *wiring function* $A^{(1)}$.

$$A^{(1)}(j) = i \quad \text{if the } j\text{-th bit of the rhythm register is wired to the } i\text{-th bit of the membrane register} \quad (2)$$

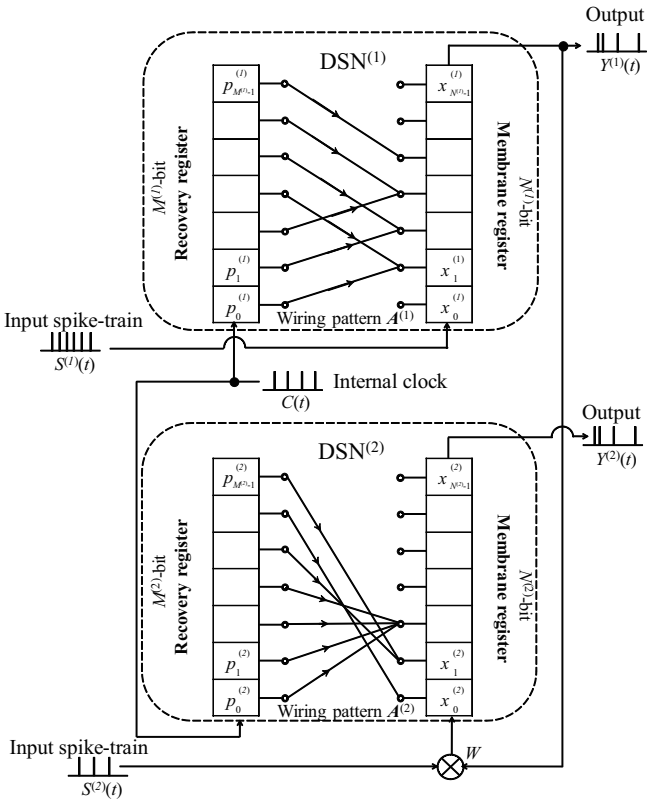

Figure 1: Pulse-coupled system of two DSNs (ab. PCDSN).

that is characterized by the following *wiring pattern* $\boldsymbol{A}^{(1)}$.

$$\boldsymbol{A}^{(1)} \equiv (A^{(1)}(0), \cdots, A^{(1)}(M^{(1)} - 1)). \tag{3}$$

Then the right terminals of the reconfigurable wires output the following one-hot-coded signal $B^{(1)}(t)$.

$$B^{(1)}(t) = A^{(1)}(P^{(1)}(t)). \tag{4}$$

The signal $B^{(1)}(t)$ is called a *base signal*. An example of the base signal $B^{(1)}(t)$ is shown in Fig.2. As shown in Fig.1, the membrane register is an $N^{(1)}$-bit one-hot-coded shift register having an integer state $X^{(1)} \in \{0, 1, \cdots, N^{(1)} - 1\}$ called a membrane potential. The DSN$^{(1)}$ accepts the following input spike-train $S^{(1)}(t)$.

$$S^{(1)}(t) = \begin{cases} 1 & \text{if } t = \phi_0^{(1)} + nd^{(1)}, \\ 0 & \text{otherwise,} \end{cases} \qquad n = 0, 1, 2, \cdots, \tag{5}$$

where $d^{(1)}$ is an input period and $\phi_0^{(1)}$ is an initial input phase. The input spike-train $S^{(1)}(t)$ induces transitions of the membrane potential $X^{(1)}(t)$ as follows.

$$X^{(1)}(t^+) = \begin{cases} X^{(1)}(t) + 1 & \text{if } S^{(1)}(t) = 1 \text{ and } X^{(1)}(t) < N^{(1)} - 1, \\ B^{(1)}(t) & \text{if } S^{(1)}(t) = 1 \text{ and } X^{(1)}(t) = N^{(1)} - 1, \\ X^{(1)}(t) & \text{otherwise.} \end{cases} \tag{6}$$

Then, as shown in Fig.2, the membrane potential $X^{(1)}(t)$ oscillates between the base signal $B^{(1)}(t)$ and the constant

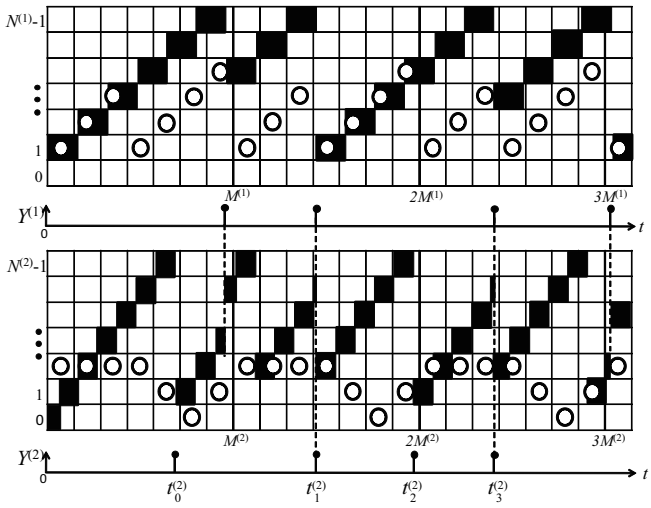

Figure 2: Time-domain waveforms of the PCDSN.

value $N^{(1)} - 1$ that can be regarded as a *firing threshold*. In addition, as shown in Fig.2, the DSN generates the following spike-train $Y^{(1)}(t)$.

$$Y^{(1)}(t) = \begin{cases} 1 & \text{if } S^{(1)}(t) = 1 \text{ and } X^{(1)}(t) = N^{(1)} - 1, \\ 0 & \text{otherwise.} \end{cases} \tag{7}$$

As shown in Fig.2, the n-th spike position in the spike-train $Y^{(1)}(t)$ is denoted by $t_n^{(1)}$ and its corresponding *spike phase* $\theta_n^{(1)}$ is defined by $\theta_n^{(1)} \equiv t_n^{(1)} \pmod{M^{(1)}} \in \boldsymbol{\Theta}^{(1)} \equiv [0, M^{(1)})$, where $n = 0, 1, 2, \cdots$. In order to characterize the spike-train $Y^{(1)}(t)$, we introduce the following definition.

Definition 1: Let a continuous closed subset $\boldsymbol{I}^{(1)}$ in the interval $\boldsymbol{\Theta}^{(1)}$ be called an *island* in $\boldsymbol{\Theta}^{(1)}$, where the interval $\boldsymbol{\Theta}^{(1)}$ is regarded as a circle (i.e., continuous at 0 and $M^{(1)}$) and thus the island $\boldsymbol{I}^{(1)}$ may include 0. Let $\{\boldsymbol{I}_0^{(1)}, \boldsymbol{I}_1^{(1)}, \cdots, \boldsymbol{I}_{Q-1}^{(1)}\}$ denote Q disjoint islands in the interval $\boldsymbol{\Theta}^{(1)}$ and let the maximum length ϵ of the islands be called an *island size*. A spike-train $Y^{(1)}(t)$ is said to be *periodic in Q-islands with size ϵ* if there exists a set of Q islands $\{\boldsymbol{I}_0^{(1)}, \boldsymbol{I}_1^{(1)}, \cdots, \boldsymbol{I}_{Q-1}^{(1)}\}$ with the island size ϵ such that $\theta_{nQ+q}^{(1)} \in \boldsymbol{I}_q^{(1)}$ for all n and q, and $\theta_{nQ+q}^{(1)} \notin \boldsymbol{I}_p^{(1)}$ for all n and $p \neq q$.

Fig.3(a) shows characteristics of the spike phase $\theta_n^{(1)}$ for the input period $d^{(1)}$, where $\{\boldsymbol{I}_0^{(1)}, \boldsymbol{I}_1^{(1)}\}$ and $\{\boldsymbol{I}_0^{(1)}, \boldsymbol{I}_1^{(1)}, \boldsymbol{I}_2^{(1)}, \boldsymbol{I}_3^{(1)}\}$ are periodic islands. In order to further characterize the spike-train $Y^{(1)}(t)$, we define the following *average inter-spike interval* (ab. average ISI) $\bar{\Delta}^{(1)}$.

$$\bar{\Delta}^{(1)} \equiv \lim_{N \to \infty} \frac{1}{N} \sum_{n=0}^{N-1} \Delta_n^{(1)}, \qquad \Delta_n^{(1)} \equiv t_{n+1}^{(1)} - t_n^{(1)}. \tag{8}$$

Fig.3(b) shows the characteristics of the average ISI.

Next, we explain the dynamics of the DSN$^{(2)}$. As shown in Fig.1, the rhythm register of the DSN$^{(2)}$ has the same structure as that of the DSN$^{(1)}$. Hence its dynamics is described by Equation (1) except that all the indexes $^{(1)}$ are

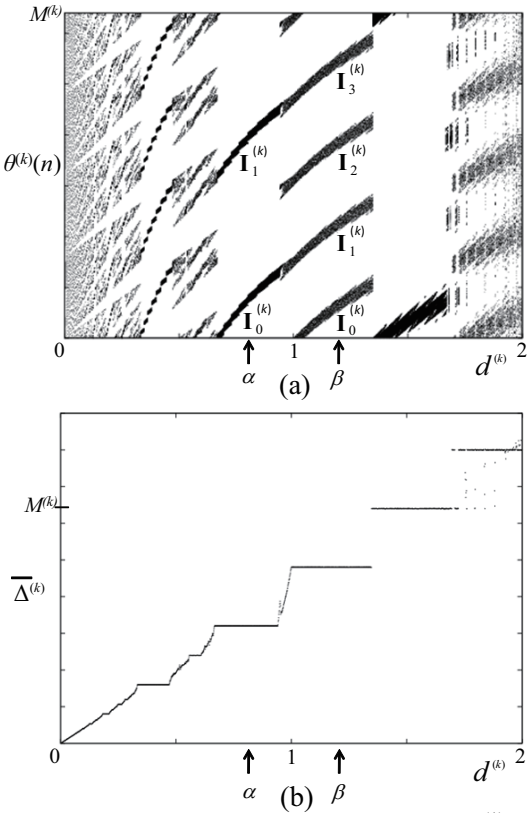

Figure 3: Bifurcation and response of the DSN$^{(1)}$ to the input $S^{(1)}(t)$. $M^{(1)} = N^{(1)} = 32$. $A^{(1)}(m) = m + 8$ for $0 \le m \le 7$, m for $8 \le m \le 15$, $m - 8$ for $16 \le m \le 23$, and $m - 16$ for $24 \le m \le 31$. (a) Bifurcation diagram of the spike phase $\theta^{(1)}(n)$. (b) Characteristics of the average ISI $\bar{\Delta}^{(1)}$.

replaced with $^{(2)}$. Also, the structure of the reconfigurable wires are the same, and thus a base signal $B^{(2)}$ of the DSN$^{(2)}$ is described by Equations (2) and (4), where all the indexes $^{(1)}$ are replaced with $^{(2)}$. As shown in Fig.1, the DSN$^{(2)}$ accepts the following input spike-train $S^{(2)}(t)$.

$$S^{(2)}(t) = \begin{cases} 1 & \text{if } t = \phi_0^{(2)} + nd^{2)}, \\ 0 & \text{otherwise,} \end{cases} \qquad n = 0, 1, 2, \cdots, \tag{9}$$

where $d^{(2)}$ is an input period and $\phi_0^{(2)}$ is an initial input phase. In addition, the DSN$^{(2)}$ accepts the spike-train $Y^{(1)}(t)$ from the DSN$^{(1)}$ through a *synaptic weight* $W \in \{-N^{(2)}, \cdots, -1, 0, 1, \cdots, N^{(2)}\}$. Then the transitions of the membrane potential $X^{(2)}(t)$ are described by the following equation.

$$X^{(2)}(t^+) = \begin{cases} X^{(2)}(t) + 1 & \text{if } S^{(2)}(t) = 1 \text{ and } X^{(2)}(t) < N^{(2)} - 1, \\ B^{(2)}(t) & \text{if } S^{(2)}(t) = 1 \text{ and } X^{(2)}(t) = N^{(2)} - 1 \text{ or} \\ & \quad Y^{(1)}(t) = 1 \text{ and } X^{(2)}(t) + W \ge N^{(2)} - 1, \\ X^{(2)}(t) + W & \text{if } Y^{(1)}(t) = 1 \text{ and } X^{(2)}(t) + W < N^{(2)} - 1, \\ X^{(2)}(t) & \text{otherwise.} \end{cases} \tag{10}$$

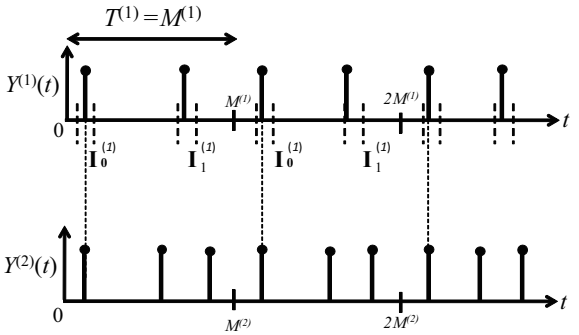

Figure 4: 2:3 locking with period $M^{(1)}$.

A typical behavior of the membrane potential $X^{(2)}$ is shown in Fig.2. As shown in this figure, the DSN$^{(2)}$ generates a spike-train

$$Y^{(2)}(t) = \begin{cases} 1 & \text{if } S^{(2)}(t) = 1 \text{ and } X^{(2)}(t) = N^{(2)} - 1 \\ & \text{or } Y^{(1)}(t) = 1 \text{ and } X^{(2)}(t) + W \ge N^{(2)} - 1, \\ 0 & \text{otherwise.} \end{cases} \tag{11}$$

and exhibits the following two types of firings.

$$\begin{array}{ll} \textit{Self-firing}: & Y^{(2)}(t) = 1 \text{ and } Y^{(1)}(t) = 0, \\ \textit{Compulsory-firing}: & Y^{(2)}(t) = 1 \text{ and } Y^{(1)}(t) = 1. \end{array}$$

In Fig.2, the DSN$^{(2)}$ exhibits self-firings at $t = t_0^{(2)}$, $t_1^{(2)}$ and $t_3^{(2)}$ and compulsory-firings at $t = t_2^{(2)}$ and $t_4^{(2)}$. In order to characterize such phenomena, we give the following definition.

Definition 2: The PCDSN is said to exhibit a $Q^{(1)}$:$Q^{(2)}$ locking with period $T^{(1)}$ and island size ϵ if (a) the DSN$^{(1)}$ generates a periodic spike-train $Y^{(1)}(t)$ in $Q^{(1)}$-islands with an island size ϵ and a period $T^{(1)}$, (b) the DSN$^{(2)}$ generates a periodic spike-train $Y^{(2)}(t)$ in $Q^{(2)}$-islands with the island size ϵ and the period $T^{(1)}$, and (c) there exists at least one island $\boldsymbol{I}_q^{(2)} \in \boldsymbol{\Theta}^{(2)}$ in which the DSN$^{(2)}$ always exhibits the compulsory-firing.

Fig.4 shows an example of 2:3 locking. In order to further characterize the lockings, we define the following *ISI ratio* ρ.

$$\rho \equiv \frac{\bar{\Delta}^{(1)}}{\bar{\Delta}^{(2)}}. \tag{12}$$

Since the DSN$^{(1)}$ and the DSN$^{(2)}$ have the common period $T^{(1)}$, the ISI ratio is given by $\rho = Q^{(2)}/Q^{(1)}$. Fig.5(a) shows numerically obtained characteristics of the ISI ratio ρ for the input period $d^{(2)}$. It can be seen in this figure that the graph of ρ is almost non-increasing and has many steps, and thus the graph is similar to the devil's staircase [15][16]. Fig.5(b) shows numerically obtained characteristics of the ISI ratio ρ for the input period $d^{(2)}$ and the synaptic weight W. It can be seen in this figure that there exist many triangular regions in which the values of the ISI ratio ρ are the same, and thus the triangular regions are similar to the Arnold tongues [15][16].

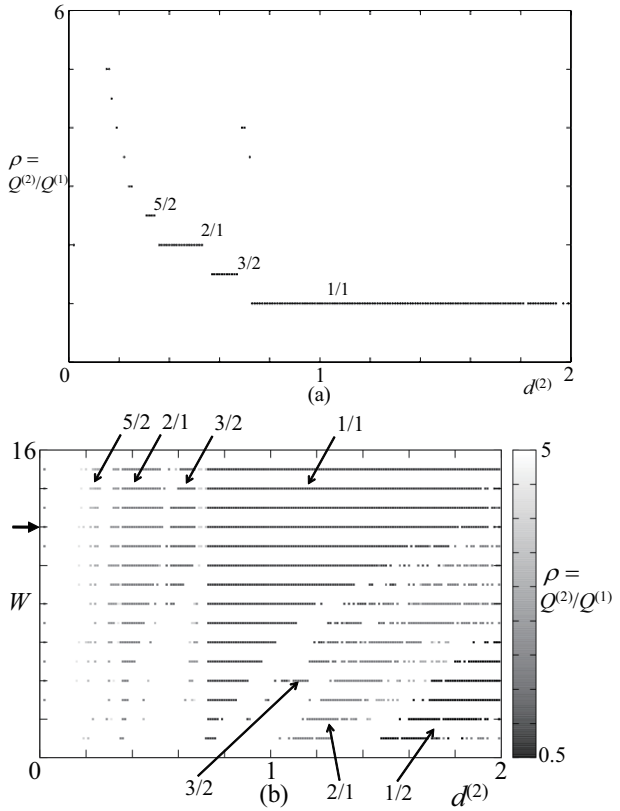

Figure 5: (a) Characteristics of the ISI ratio ρ for the input period $d^{(2)}$ to the DSN$^{(2)}$, where the input period $d^{(1)} = 0.78$ to the DSN$^{(1)}$ is fixed. The parameter values of the DSN$^{(1)}$ are same as those in Fig.3. The parameter values of the DSN$^{(2)}$ are $M^{(2)} = M^{(1)}$, $N^{(2)} = N^{(1)}$, and $A^{(2)}(m) = A^{(1)}(m)-2$ for $m = 0, 1, \cdots, M^{(1)}-1$. The synaptic weight is $W = 12$. (b) Characteristics of the ISI ratio ρ for $d^{(2)}$ and W. The parameter values of the PCDSN and the input period $d^{(1)}$ are identical with those in (a) except for the synaptic weight W.

3. Conclusions

The one-way pulse-coupled system of two integrate-and-fire type digital spiking neurons was introduced. It was shown that the pulse-coupled system can exhibit various periodic synchronizations whose characteristics have certain degrees of similarities to devil's staircases and Arnold tongues. Future problems include the following points: (a) more detailed analysis of synchronization phenomena of the PCDSN; (b) synthesis and analysis of a large-scale network of DSNs; and (c) development of an on-FPGA learning method for the large-scale network to mimic spatiotemporal phenomena of a local circuit of the brain. The authors would like to thank Professor Toshimitsu Ushio of Osaka University for valuable discussions. This work is partially supported by the Center of Excellence for Founding Ambient Information Society Infrastructure, Osaka University, Japan, and KAKENHI (21700253).

References

[1] C. Mead and M. Ismail, Analog VLSI implementation of neural systems, Springer, 1989.

[2] W. Maass and C. Bishop, Pulsed neural networks, Bradford Book, 1999.

[3] T. Kohno and K. Aihara, A MOSFET-based model of a class 2 nerve membrane, IEEE Trans. Neural Networks, Vol. 16, No. 3, pp.754-773, 2005.

[4] K. Kinoshita and H. Torikai, A self-organizing pulse-coupled network of sub- threshold oscillating spiking neurons, IEICE Trans. Fundamentals, Vol.E94-A, No.1, pp.300-314, 2011.

[5] H. Torikai and T. Nishigami, An artificial chaotic spiking neuron inspired by spiral ganglion cell: Paralleled spike encoding, theoretical analysis, and electronic circuit implementation, Neural Networks Vol. 22, pp. 664-673, 2009.

[6] T. Massoud and T. Horiuchi, A Neuromorphic VLSI Head Direction Cell System, IEEE Trans. CAS-I, vol. 58, no. 1, pp. 150–163, 2011.

[7] T. Schoenauer *et al.*, NeuroPipe-Chip: A digital neuroprocessor for spiking neural networks, IEEE Trans. Neural Networks, vol. 13, no. 1, pp. 205 –213, Jan. 2002.

[8] T. Matsubara, H. Torikai and T. Hishiki, A Generalized Rotate-and-Fire Digital Spiking Neuron Model and its On-FPGA Learning, IEEE Trans. CAS-II, 2011 (accepted).

[9] T. Hishiki and H. Torikai, A Novel Rotate-and-Fire Digital Spiking Neuron and its Neuron-like Bifurcations and Responses, IEEE Trans. Neural Networks, Vol. 22, No. 5, pp. 752-767, 2011.

[10] S. Hashimoto and H. Torikai, A novel hybrid spiking neuron: Bifurcations, Responses, and On-chip learning, IEEE Trans. Circuits and Systems part I, Vol.57, No.8, pp.2168-2181, 2010.

[11] H. Ijichi and H. Torikai, Theoretical Analysis of Various Synchronizations in Pulse-Coupled Digital Spiking Neurons, Proc. International Conference on Neural Information Processing, pp.107-115, 2010.

[12] Xilinx's FPGAs Virtex-5, 6, and 7 support the dynamic reconfiguration (http://www.xilinx.com/).

[13] L. O. Chua, A Nonlinear Dynamics Perspective of Wolfram's New Kind of Science, vol.1–3, World Scientific Pub., 2007.

[14] Mark Zwolinski, Digital System Design with VHDL, 2nd Edition, Prentice Hall, 2004.

[15] E. Ott, Chaos in dynamical systems, Cambridge University Press, 1993.

[16] R. Devaney, An introduction to chaotic dynamical systems, Westview Press, 2003.